

Synthesis, characterization, and *in silico* analysis against SARS CoV-2 of novel benzimidazolium salts

Elvan ÜSTÜN*¹ and Neslihan ŞAHİN²

¹Department of Chemistry, Faculty of Art and Science, Ordu University, 52200, Ordu, Turkey

²Department of Basic Education, Faculty of Education, Cumhuriyet University, 58140, Sivas, Turkey

Abstract. In acute conditions, vaccines are very important, although they provide antibodies for fighting against COVID-19 for a certain period. It is necessary to produce an anti-viral agent for a usual healing process against SARS CoV-2 which is responsible the pandemic we are living in. Many drugs with benzimidazole main scaffold are still used in a wide variety of treatment procedures. In this case, substituted benzimidazole structures could be good candidates for fighting against COVID-19. Theoretical calculation methods could be a key tool for overcome the difficulties of individual analyzing of each new structure. In this study, new benzimidazole structures were synthesized and characterized for *in silico* evaluation as anti-viral agent. The molecules were optimized and analyzed for reactivity with Koopmans Theorem. Also, molecular docking simulations were performed for SARS coronavirus main peptidase (PDB ID: 2GTB), COVID-19 main protease (PDB ID: 5R82), and papain-like protease of SARS CoV-2 (PDB ID: 6W9C) crystals.

Keywords: benzimidazolium; molecular docking; COVID-19; global reactivity descriptors.

1. Introduction

SARS CoV-2 is responsible for the largest pandemic that the current generation has ever seen [1]. According to the data of the World Health Organization [14.12.2021], 269.468.311 confirmed cases of COVID-19, including 5.304.248 deaths were recorded [2]. The recent fighting against the pandemic continues with vaccination. Considering the temporality of vaccine protection and the difficulties in reaching the vaccine for the world population, it is clear that anti-viral drugs have to be developed [3]. The scientists have examined the anti-viral effects of many current molecules and tried to design more active new molecules [4-6]. However, it is not possible to analyze all synthetic and natural antiviral known or candidate molecules with the current budget, labor, and lab conditions. Considering the recent developments in computational chemistry and the high compatibility of the results with experimental results, theoretical chemistry has presented important foresights in performing these studies with current possibilities [7, 8].

Woolley confirmed that benzimidazole derivative molecules show purine-like activity [9]. Benzimidazole main scaffold can be modified easily with different substituents [10]. The studies that investigating the activity of benzimidazole molecules with different substituents are frequently encountered such as antimicrobial, antiparasitic, antiviral, anticancer, anti-inflammatory [11-15]. Albendazole, omeprazole, lansoprazole, astemizole and telmisartan are benzimidazole derivative molecules currently used in treatment procedures [16, 17]. In this case, the

benzimidazole derivative molecules can be examined in the fight against the SARS CoV-2 virus.

Theoretical computational chemistry provides useful information for studying the activity of molecules. Information that provides preliminary evaluation about the activities of molecules saves labor and money in experimental analysis. In addition, since the obtained insights prevent the analysis of relatively more passive molecules, it prevents the contact of harmful chemicals used during the experimental procedure with humans and nature. Recently, there have been important developments in this area. Thanks to these developments, non-synthesized molecules can be analyzed, and methods such as molecular docking are accepted as essential tools in drug design studies [18].

In this study, 1-allyl-3-(2-methylbenzyl)-5,6-dimethylbenzimidazolium chloride (**1**), 1-allyl-3-(3-methylbenzyl)-5,6-dimethylbenzimidazolium chloride (**2**), and 1-allyl-3-(4-methylbenzyl)-5,6-dimethylbenzimidazolium chloride (**3**) were synthesized and fully characterized by FT-IR, ¹H NMR and, ¹³C{¹H} NMR spectroscopies. Their structures were optimized by DFT-based calculation method by using the exchange functional BP86 with TZV basis set, HOMO (Highest Occupied Molecular Orbital) and LUMO (Lowest Unoccupied Molecular Orbital) were analyzed, and Global Reactivity Descriptors of the molecules were determined by Koopmans Theorem [19]. Also, the interactions of the molecules were evaluated with SARS coronavirus main peptidase (PDB ID: 2GTB), COVID-19 main protease (PDB ID: 5R82), and papain-like protease of SARS CoV-2 (PDB ID: 6W9C) by molecular docking methods [20-23].

* Corresponding author. *E-mail address:* elvanustun77@gmail.com (Elvan Üstün)

2. Experimental

2.1. Materials and methods

All experiments were performed under argon in flame-dried glassware using standard Schlenk line techniques. All reagents were purchased from Sigma Aldrich Co. (Dorset, UK). The solvents used were purified by distillation over the drying agents indicated and were transferred under argon. Melting points were determined using the Electrothermal 9100 melting point detection apparatus in capillary tubes and the melting points are reported as uncorrected values. Fourier transform infrared (FT-IR) spectra were recorded in the range of 400–4000 cm^{-1} on Perkin Elmer Spectrum 100 FT-IR. ^1H NMR and $^{13}\text{C}\{^1\text{H}\}$ NMR spectra were taken using a Bruker As 400 Mercury spectrometer operating at 400 MHz (^1H), 100 MHz (^{13}C) in CDCl_3 with tetramethylsilane as the internal reference. ^1H peaks are labeled as singlet (s).

2.2. General procedure for the preparation of N-heterocyclic carbene salts

The N-heterocyclic carbene salts (**1-3**) were synthesized under argon gas atmosphere and according to the literature [24].

1-Allyl-3-(2-methylbenzyl-5,6-dimethylbenzimidazolium chloride, **1**)

To a stirring solution of NaH (11 mmol) in tetrahydrofuran (20 mL), 5,6-dimethylbenzimidazole (10 mmol) was added and admixture was stirred at room temperature for 1 h. Then, allyl bromide (10.1 mmol) was added to the solution and the mixture was left to stir for 24 h at 60 °C. The mixture was cooled to room temperature. Then, the solvent was removed in vacuo. Dichloromethane (30 mL) was added to solid. The last solution was distilled and 1-allyl-5,6-dimethylbenzimidazole was obtained. The 1-allyl-5,6-dimethylbenzimidazole (1 mmol) and 2-methylbenzyl chloride (1 mmol) were stirred in DMF (5 mL) for 24 h at 80 °C. Precipitated solid was filtered and rinsed out with diethyl ether and dried under vacuum. Yield: 88%; m.p. 215-216 °C, FT-IR $\nu_{(\text{CN})}$: 1557 cm^{-1} . ^1H NMR (400 MHz, CDCl_3) δ (ppm): 2.33 (s, 3H, $\text{CH}_2\text{C}_6\text{H}_4\text{-CH}_3\text{-2}$), 2.41, 2.42 (s, 6H, $\text{NC}_6\text{H}_2\text{N}(\text{CH}_3)_2\text{-5,6}$), 5.31 (d, 2H, $\text{NCH}_2\text{CHCH}_2$, $J = 8$ Hz), 5.41-5.47 (m, 2H, $\text{NCH}_2\text{CHCH}_2$), 5.83 (s, 2H, $\text{CH}_2\text{C}_6\text{H}_4\text{-CH}_3\text{-2}$), 6.11 (quint, 1H, $\text{NCH}_2\text{CHCH}_2$, $J = 4$ Hz), 7.02 (d, 2H, Ar-H, $J = 4$ Hz), 7.14-7.19 (m, 2H, Ar-H), 7.24-7.29 (m, 2H, Ar-H), 11.69 (s, 1H, NCHN). $^{13}\text{C}\{^1\text{H}\}$ NMR (100 MHz, CDCl_3) δ (ppm): 19.6 ($\text{CH}_2\text{C}_6\text{H}_4\text{-CH}_3\text{-2}$), 20.7 ($\text{NC}_6\text{H}_2\text{N}(\text{CH}_3)_2\text{-5,6}$), 49.7 ($\text{CH}_2\text{C}_6\text{H}_4\text{-CH}_3\text{-2}$), 50.0 ($\text{NCH}_2\text{CHCH}_2$), 126.8 ($\text{NCH}_2\text{CHCH}_2$), 136.4 ($\text{NCH}_2\text{CHCH}_2$), 113.2, 113.4, 121.3, 127.8, 129.2, 129.9, 130.0, 130.1, 130.8, 131.3 (Ar-C), 143.2 (NCHN).

1-Allyl-3-(3-methylbenzyl-5,6-dimethylbenzimidazolium chloride, **2**)

2 was prepared following the same procedures as described for **1**. However, 3-methylbenzyl chloride (1 mmol) was used as second added alkyl halide. Yield: 85%; m.p. 228-229 °C, FT-IR $\nu_{(\text{CN})}$: 1561 cm^{-1} . ^1H NMR (400 MHz, CDCl_3) δ (ppm): 2.33 (s, 3H, $\text{CH}_2\text{C}_6\text{H}_4\text{-CH}_3\text{-3}$), 2.38, 2.41 (s, 6H, $\text{NC}_6\text{H}_2\text{N}(\text{CH}_3)_2\text{-5,6}$), 5.28 (d, 2H, $\text{NCH}_2\text{CHCH}_2$, $J = 8$ Hz), 5.42-5.46 (m, 2H,

$\text{NCH}_2\text{CHCH}_2$), 5.77 (s, 2H, $\text{CH}_2\text{C}_6\text{H}_4\text{-CH}_3\text{-3}$), 6.11 (quint, 1H, $\text{NCH}_2\text{CHCH}_2$, $J = 4$ Hz), 7.15 (s, 1H, Ar-H), 7.24-7.26 (m, 3H, Ar-H), 7.30-7.31 (m, 1H, Ar-H), 7.41 (s, 1H, Ar-H), 11.75 (s, 1H, NCHN). $^{13}\text{C}\{^1\text{H}\}$ NMR (100 MHz, CDCl_3) δ (ppm): 20.7 ($\text{NC}_6\text{H}_2\text{N}(\text{CH}_3)_2\text{-5,6}$), 21.4 ($\text{CH}_2\text{C}_6\text{H}_4\text{-CH}_3\text{-3}$), 50.0 ($\text{CH}_2\text{C}_6\text{H}_4\text{-CH}_3\text{-3}$), 51.3 ($\text{NCH}_2\text{CHCH}_2$), 125.1 ($\text{NCH}_2\text{CHCH}_2$), 132.9 ($\text{NCH}_2\text{CHCH}_2$), 113.2, 113.4, 121.4, 128.7, 129.2, 129.9, 130.0, 137.3, 137.4, 139.3 (Ar-C), 142.6 (NCHN).

1-Allyl-3-(4-methylbenzyl-5,6-dimethylbenzimidazolium chloride, **3**)

3 was prepared following the same procedures as described for **1**. However, 4-methylbenzyl chloride (1 mmol) was used as second added alkyl halide. Yield: 89%; m.p. 210-211 °C, FT-IR $\nu_{(\text{CN})}$: 1558 cm^{-1} . ^1H NMR (400 MHz, CDCl_3) δ (ppm): 2.24 (s, 3H, $\text{CH}_2\text{C}_6\text{H}_4\text{-CH}_3\text{-4}$), 2.31, 2.33 (s, 6H, $\text{NC}_6\text{H}_2\text{N}(\text{CH}_3)_2\text{-5,6}$), 5.22 (d, 2H, $\text{NCH}_2\text{CHCH}_2$, $J = 8$ Hz), 5.35-5.39 (m, 2H, $\text{NCH}_2\text{CHCH}_2$), 5.71 (s, 2H, $\text{CH}_2\text{C}_6\text{H}_4\text{-CH}_3\text{-4}$), 6.06 (quint, 1H, $\text{NCH}_2\text{CHCH}_2$, $J = 4$ Hz), 7.08-7.16 (m, 2H, Ar-H), 7.28-7.37 (m, 4H, Ar-H), 11.36 (s, 1H, NCHN). $^{13}\text{C}\{^1\text{H}\}$ NMR (100 MHz, CDCl_3) δ (ppm): 20.7 ($\text{NC}_6\text{H}_2\text{N}(\text{CH}_3)_2\text{-5,6}$), 21.2 ($\text{CH}_2\text{C}_6\text{H}_4\text{-CH}_3\text{-4}$), 50.0 ($\text{CH}_2\text{C}_6\text{H}_4\text{-CH}_3\text{-4}$), 51.1 ($\text{NCH}_2\text{CHCH}_2$), 128.2 ($\text{NCH}_2\text{CHCH}_2$), 137.3 ($\text{NCH}_2\text{CHCH}_2$), 113.2, 113.4, 121.3, 129.9, 130.0, 130.1, 139.0 (Ar-C), 142.3 (NCHN).

2.3. Calculation method

Full unconstrained geometry optimizations with DFT-based calculation methods were carried out with ORCA version 2.8 using the exchange functional according to BP86 that the correlation functional suggested by Becke and Perdew, with the resolution-of-the-identity (RI) approximation, the tightscf and grid4 options, a TZV basis set [25, 26]. Scalar relativistic effects were treated using the Zeroth Order Regular Approximation (ZORA) formalism [27-29]. To speed up the calculations TZV/J auxiliary basis set was used [30]. All the global chemical reactivity descriptors were calculated with Koopmans Theorem according to following equations [31]:

$$IP = -E_{HOMO} \quad (1)$$

$$EA = -E_{LUMO} \quad (2)$$

$$\chi = -\frac{I + A}{2} \quad (3)$$

$$\eta = \frac{I - A}{2} \quad (4)$$

$$S = \frac{1}{2\eta} \quad (5)$$

$$\omega = \frac{\mu^2}{2\eta} \quad (6)$$

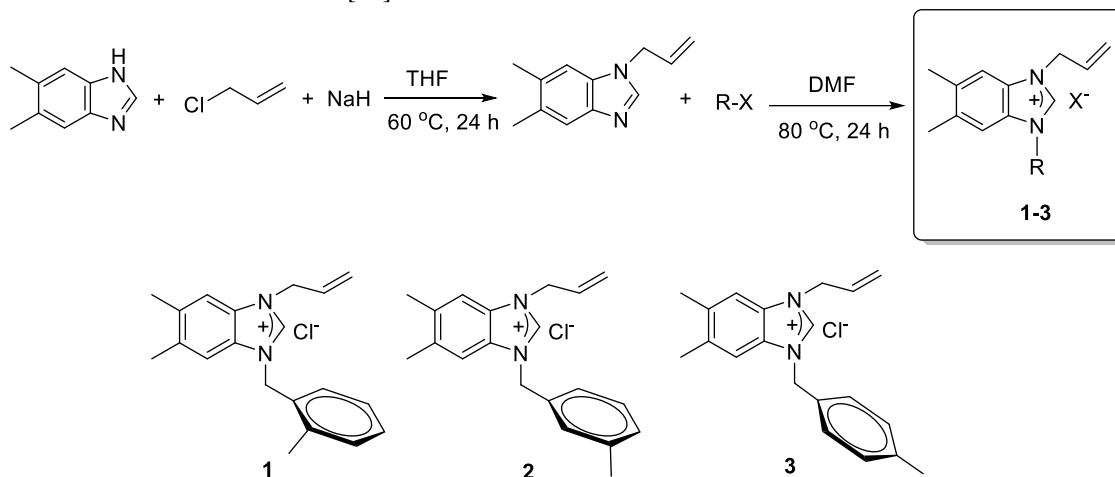
AutoDockTools 4.2 were used for molecular docking calculations [32] with crystal structure from RCSB protein data bank (PDB ID: 2GTB, 5R82, 6W9C). Only polar hydrogens and Kollman charges were evaluated in target molecules and the waters in proteins were removed [33]. Randomized starting positions, Gasteiger charges, torsions have been

evaluated for ligand molecules [34]. While Lamarkian genetic algorithms were applied, the genetic algorithm population was recorded as 150 [35]. The grids were selected as 60/60/56 npts with 4.754/1.384/14.716 (x/y/z) for 2GTB; 66/78/96 npts with 9.938/-3.465/8.302 (x/y/z) for 5R82; and 52/110/68 npts with -26.273/34.465/31.382 (x/y/z) for 6W9C. Discovery Studio 4.1.0 were used for illustrations [36].

3. Results and discussion

3.1. Characterization of N-heterocyclic carbene salts

N-heterocyclic carbene salts (**1-3**) were synthesized as shown Scheme 1.



Scheme 1. Synthesis of N-heterocyclic carbene salts (**1-3**)

N-heterocyclic carbene salts were synthesized by reaction of allyl substituted benzimidazolium precursor with different alkyl halides in DMF at 80 °C. Precipitated product was crystallized in dichloromethane/diethyl ether for purification. The structure of all new compounds was characterized by FT-IR, ^1H NMR and $^{13}\text{C}\{^1\text{H}\}$ NMR spectroscopy.

The FT-IR spectra for all NHC salts (**1-3**) showed the aliphatic and aromatic C-H stretching vibrational bands in the range of 3100-2700 cm^{-1} . C=C stretching vibration modes of all compounds were seen at around 1700-1600 cm^{-1} . Benzimidazole ring C=N vibrations of benzimidazolium salts were assigned at 1557, 1561 and 1558 cm^{-1} for **1-3**, respectively.

NMR spectra of all the compounds were analyzed in deuteriochloroform (d-CDCl_3). In the ^1H NMR spectra, acidic protons (NCHN) for N-heterocyclic carbene salts (**1-3**) were seen as a characteristic sharp singlet at 11.69, 11.75 and 11.36 ppm respectively. Methyl protons in the benzyl and 5,6-dimethylbenzimidazole groups came around 2.24-2.42 ppm for **1-3**. Alkyl protons in **1-3** gave peaks around 5.22-5.83 ppm. Middle protons of $\text{NCH}_2\text{CHCH}_2$ came at 6.11, 6.11 and 6.06 ppm as a quint respectively. All aromatic protons were seen in the range of 7.00-7.45 ppm for **1-3** compounds. In the $^{13}\text{C}\{^1\text{H}\}$ NMR spectra, aromatic carbons in **1-3** compounds were detected in the range of 113.0-140.0 ppm. NCHN carbon on **1-3** salts signaled at 143.2, 142.6 and 142.3 ppm, respectively. Benzylic carbons of benzyl groups were observed at 49.7, 50.9 and 50.0 ppm for **1-3**, respectively. Observed peaks in the range of 19.0-22.0 ppm were attributed to all methyl carbons. These values agree with reported data for similar N-heterocyclic carbenes [37]. The FT-IR, ^1H NMR and, $^{13}\text{C}\{^1\text{H}\}$ NMR spectra are presented in the details in the Supplementary Files (Figures S1, S6).

3.2. DFT-based analysis and molecular docking

In this study, the optimizations of the molecules were performed with ORCA package. HOMO and LUMO analysis of the molecules are important since these orbitals are the most reactive area of the molecules [38]. HOMO is defined that the molecules behave through as a Lewis acid while LUMO residue also act as Lewis base [39]. According to the optimization results, it has been determined that the HOMO is located on benzyl part, and also LUMO is resided on benzimidazole main scaffold (Figure 1).

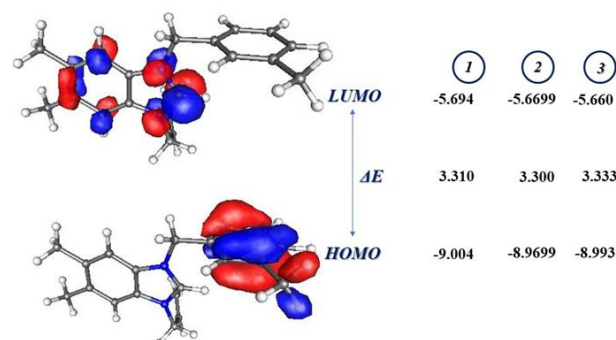


Figure 1. HOMO and LUMO energies and illustrations of the molecules (in eV)

Also, the higher HOMO-LUMO gap energy, the lower chemical reactivity, and the higher kinetic stability. According to the calculated HOMO-LUMO gap energies of the investigated molecules, the most reactive molecule is **2**, while **3** has the most kinetic stability. Moreover, HOMO energies are evaluated as a measurement of the Ionization Potential of molecules while LUMO energies are also evaluated for Electron Affinity of the molecules. On the other hand, Global Reactivity Descriptors of Koopmans Theorem allow to relative analysis of the reactivity of the molecules [40].

These descriptors in this study shows that **1** has the highest ionization potential. In addition, global softness and chemical hardness are also approved as evaluation criteria for the reactivity of molecules. The stability of molecules decreases with the increasing of the global softness, so the higher the hardness, the lower the reactivity [41]. It is clear from Table 1 that the reactivity of the molecules will be listed as $2 > 1 > 3$. Electrophilicity index is regarded as an indication of the electrophilic force of the molecular system against a nucleophile [42].

Table 1. Global reactivity descriptors of the complexes (in eV)

	1	2	3
Ionization Potential (IP)	9.004	8.970	8.993
Electron Affinity (EA)	5.694	5.670	5.660
Electronegativity (χ)	7.349	7.320	7.326
Global Softness (S)	0.302	0.303	0.300

	1	2	3
Global Hardness (η)	1.655	1.650	1.667
Electrophilicity Index (ω)	16.310	16.235	16.101

COVID-19 continues to affect all the world as the biggest pandemic faced by the living generation. In the acute situation, the priority has focused on vaccination studies in order to prevent deaths. Considering the limited time of action of the vaccine and the difficulties in vaccine dissemination for fully protection, drug design studies should be focused on in fighting against the disease. Recently, the activity of many synthetic and natural molecules against COVID-19 has been studied. Considering the difficulty of analyzing the anti-viral activity of all known and newly synthesized molecules, studies with in-silico methods have become important. Now, it is possible to see molecular docking studies performed against many crystals. In this study, three certain crystal structures were used.

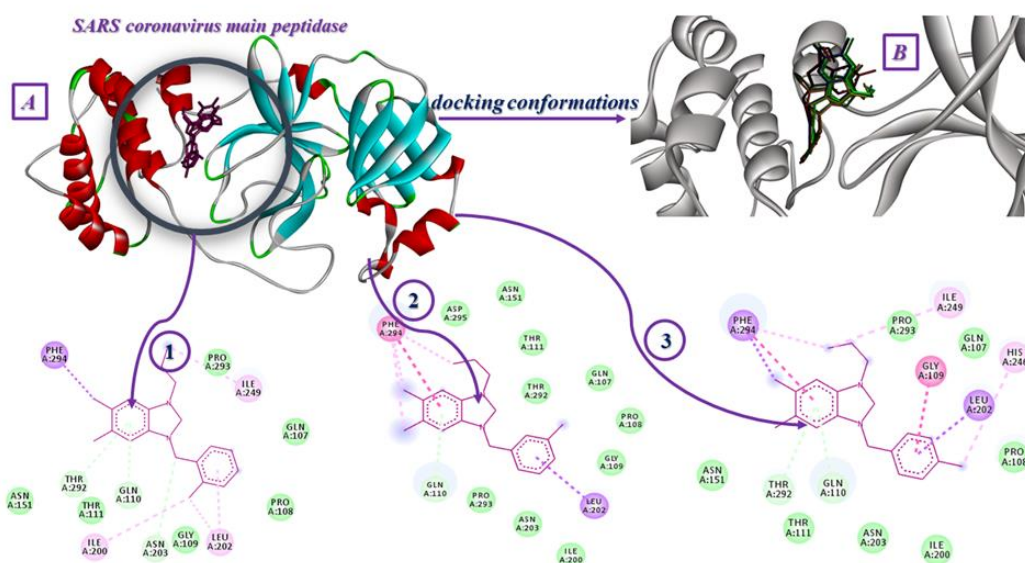


Figure 2. Interaction residue (A: PDB fragment 2GTB [21]), docking conformations (B) and interaction type of benzimidazole type **1**, **2**, and **3** with SARS coronavirus main peptidase crystal structure (dark green and turquoise: H-bonds; green: van der Waals; orange: π -anion/cation; pink: alkyl and π -alkyl; yellow: π -sulfur; fuchsia: π - π stacked and π - π T shaped)

In the first study, three optimized benzimidazole derivative molecules were interacted with SARS coronavirus main peptidase [21]. All molecules interacted with approximately the same region of the crystal (Figure 2). According to the obtained results, the H-bonds with the residue of included Phe294, Pro293, Gln107, Gln110 and Asn151 amino acids were recorded for all three molecules (Figure 2, A). H-bonds with Gln110, Asn203, and Thr292, π -sigma interaction with Phe294 and alkyl/ π -alkyl interactions with Ile200, Leu202 and Ile249 have been recorded. The molecule is interacted with crystal in one type of conformation, no difference is noted in the orientation of the molecule. The calculated binding energies for **1** and **3** are equal with -6.07 kcal/mol. H-bond with Gln110 and Thr292 and π - π stacked interactions with Phe294 and Leu202 and π - π stacked interactions with Gly109 for **3** could be effective in calculated binding energy. The interactions of alkyl/ π -alkyl with His246 and Ile249 are also recorded. Although the binding energy of **2** was determined as -6.06 kcal/mol, only one H-bond was detected with Gln110. Phe294 is remarkable in this

docking pose with both π - π stacked and alkyl/ π -alkyl interactions. Salim and Nouredine performed molecular docking for reference inhibitor AZP (PubChem Code: 5287723) against SARS coronavirus main peptidase and determined -7.499 kcal/mol as binding constant that is higher than the that of 1-3. They also analyzed the interactions for some well-known anti-viral drugs such as remdesivir (-7.079 kcal/mol), favipiravir (-4.122 kcal/mol) and hydroxychloroquine (-5.515 kcal/mol) [43]. We also docked favipiravir, hydroxychloroquine, nelfinavir, remdesivir, and lopinavir into SARS coronavirus main peptidase with our protocol. Binding affinities were recorded -3.66 kcal/mol for favipiravir, -5.24 kcal/mol for hydroxychloroquine, -4.15 kcal/mol for remdesivir, -5.12 kcal/mol for nelfinavir, and -6.2 kcal/mol for lopinavir. The molecules that studied in this research gives better score and could be a suitable inhibitor for SARS coronavirus main peptidase.

Among the crystal structures used in this study, the highest binding values were determined with the COVID-19 main protease structure [22]. The binding

energies between the crystal and **1**, **2**, and **3** were determined as -8.64 kcal/mol, -8.72 kcal/mol and -7.77 kcal/mol, respectively. H-bonds with Arg298 and Val303 can be considered as effective in **2** which have the highest binding energy. In addition, it can be determined that the interactions of π - cation with Arg298, π - sulfur with Met6, π -sigma and π - π T-shaped with Phe8 are effective. It can be seen in Figure 3 that these amino acids are also have alkyl and π - alkyl interactions. On the other hand, many Van der Waals interactions have also been recorded. Al-Zahrani were docked many phytochemicals, some known anti-viral drugs and also reference inhibitor (RZS, 6-(ethylamino)pyridine-3-carbonitrile) against COVID-19 main protease [44]. The research recorded -4.90 kcal/mol, -8.40 kcal/mol, -7.90 kcal/mol binding constant for RZS, lopinavir, and nelfinavir, respectively.

Both **1** and **2** have better binding score than reference inhibitor and the drugs while **3** have better binding constant than only reference inhibitor. The interaction residues that we determined for 1-3 are compatible with the active sites of the COVID-19 main protease that recorded by Al-Zahrani. Some FDA-approved drugs were docked into COVID-19 main protease crystal and the binding constants of favipiravir, hydroxychloroquine, nelfinavir, remdesivir, and lopinavir were detected as -5.29 kcal/mol, -5.17 kcal/mol, -7.85 kcal/mol, -6.02 kcal/mol, and -3.89 kcal/mol, respectively. The molecules that studied in this research have bigger binding score than these approved drugs and these results could be an indication for being a suitable inhibitor for COVID-19 main protease.

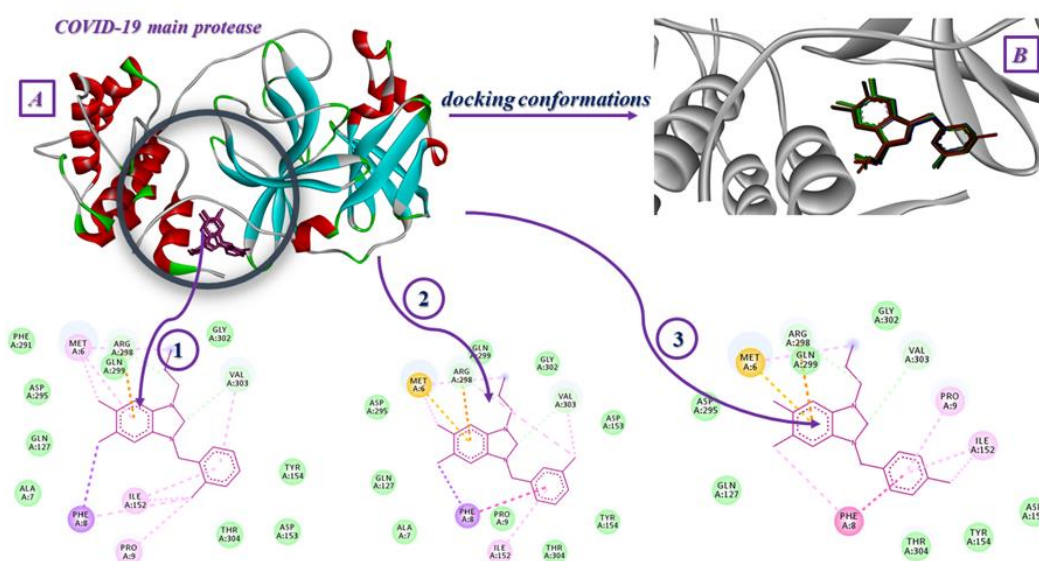


Figure 3. Interaction residue (A: PDB fragment 5R82 [22]), docking conformations (B) and interaction type of benzimidazole type **1**, **2**, and **3** with COVID-19 main protease crystal structure (dark green and turquoise: H-bonds; green: van der Waals; orange: π - anion/cation; pink: alkyl and π - alkyl; yellow: π -sulfur; fuchsia: π - π stacked and π - π T shaped)

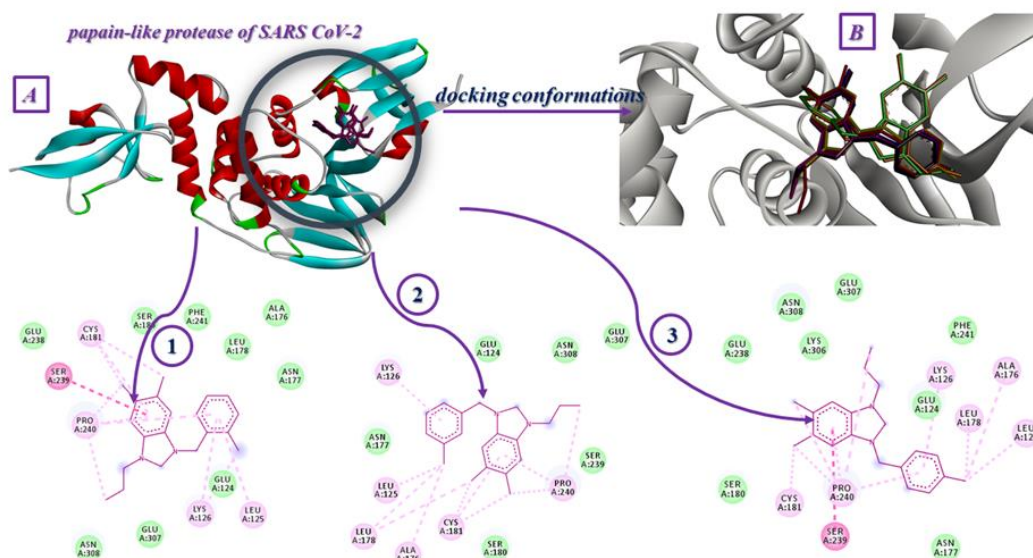


Figure 4. Interaction residue (A: PDB fragment 6W9C [23]), docking conformations (B) and interaction type of benzimidazole type **1**, **2**, and **3** with papain-like protease of SARS CoV-2 crystal structure (dark green and turquoise: H-bonds; green: van der Waals; orange: π - anion/cation; pink: alkyl and π - alkyl; yellow: π -sulfur; fuchsia: π - π stacked and π - π T shaped)

Recently, papain-like protease has been used frequently in *in silico* COVID-19 studies. Papain-like protease [23] is effective in virus replication and maturation. Strong interactions with this crystal could be important for the candidate molecule. In this study, all the molecules interact with approximately the same region of the crystal. Unlike other crystals, two different molecular orientations were determined. The binding energies of the molecules evaluated in this study with papain-like protease were determined as -5.63 kcal/mol, -5.70 kcal/mol and -5.38 kcal/mol. The strongest binding energy was determined for **2**. No interaction was noted in these poses except alkyl/ π -alkyl and van der Waals. There is an amide - π stacked interaction with Ser239 for **1** and **3**, but it is not having a big effect on total binding energy. All interaction details of molecules can be analyzed in Figure 4. Papain-like protease of SARS CoV-2 were also interacted with some FDA-approved drugs with molecular docking method. The binding constants of favipiravir, hydroxychloroquine, nelfinavir, remdesivir, and lopinavir were calculated as -4.88 kcal/mol, -4.20 kcal/mol, -5.09 kcal/mol, -3.17 kcal/mol, and -3.31 kcal/mol, respectively. These results could represent that the benzimidazolium salts could be an inhibitor for papain-like protease of SARS CoV-2.

4. Conclusions

Benzimidazole derivative molecules are still used effectively in many treatment procedures. Therefore, it is important to examine the effect of these molecules on the pandemic that is still happening. These analyses have been carried out with molecular docking methods, which are considered important tool in drug design studies recently. The strongest binding energies in the study were obtained with COVID-19 main protease. Also, good binding scores were determined SARS coronavirus main peptidase and papain-like protease. Some of the binding constants of the characterized molecules are better than some of well-known anti-viral drug molecules and this means that these molecules could be better inhibitor than some of commercial anti-viral compounds. It may be suggested to extend the work through more efficient substituents, such as the halogenic species. It is also known that this family makes effective complexes with many transition metals. Examining the effect of different metals on the virus can be evaluated in future studies.

Conflict of interest

The authors declare that they have no known competing financial interests or personal relationships that could have appeared to influence the work reported in this paper.

References

- [1]. D. Wu, T. Wu, Q. Liu, Z. Yang, The SARS-CoV-2 outbreak: What we know, *International Journal of Infectious Diseases* 94 (2020) 44-48. Doi: 10.1016/j.ijid.2020.03.004
- [2]. <https://covid19.who.int/> "visited in 14.12.2021"
- [3]. J.A. Singh, COVID-19 vaccine trials: Duty of care and standard of prevention considerations, *Vaccine* 38 (2020) 7578–7580. Doi: 10.1016/j.vaccine.2020.10.012
- [4]. V. Gies, N. Bekaddour, Y. Dieudonné, A. Guffroy, Q. Frenger, F. Gros, M. P. Rodero, J.P. Herbeuval, A.S. Korganow, Beyond Anti-viral Effects of Chloroquine/Hydroxychloroquine, *Front. Immunol.* 11 (2020) 1409. Doi: 10.3389/fimmu.2020.01409
- [5]. L. Runfeng, H. Yunlonge, H. Jicheng, P. Weiqi, M. Qin Hai, S. Yongxia, L. Chufang, Z. Jin, J. Zhenhua, J. Haiming, Z. Kui, H. Shuxiang, D. Jun, L. Xiaobo, H. Xiaotao, W. Lin, Z. Nanshan, Y. Zifen, Lianhuaqingwen exerts anti-viral and anti-inflammatory activity against novel coronavirus (SARS-CoV-2), *Pharmacological Research* 156 (2020) 104761. Doi: 10.1016/j.phrs.2020.104761
- [6]. E. Teirumnieks, I. Balchev, R.S. Ghalot, L. Lazov, Antibacterial and anti-viral effects of silver nanoparticles in medicine against COVID-19—a review, *Laser Phys.* 31 (2021) 013001. Doi: 10.1088/1555-6611/abc873
- [7]. J. Xu, L. Gao, H. Liang, S. Chen, In silico screening of potential anti-COVID-19 bioactive natural constituents from food sources by molecular docking, *Nutrition* 82 (2021) 111049. Doi: 10.1016/j.nut.2020.111049
- [8]. A.B. Gumel, E.A. Iboi, C.N. Ngonghala, E.H. Elbash, A primer on using mathematics to understand COVID-19 dynamics: Modeling, analysis and simulations, *Infectious Disease Modelling* 6 (2021) 148-168. Doi: 10.1016/j.idm.2020.11.005
- [9]. M. Kubeil, R.R. Vernooij, C. Kubeil, B.R. Wood, B. Graham, H. Stephan, L. Spiccia, Studies of Carbon Monoxide Release from Ruthenium(II) Bipyridine Carbonyl Complexes upon UV-Light Exposure, *Inorganic Chemistry* 56 (2017) 5941–5952. Doi: 10.1021/acs.inorgchem.7b00599
- [10]. Y. Wang, K. Sarris, D.R. Sauer, S.W. Djuric, A simple and efficient one step synthesis of benzoxazoles and benzimidazoles from carboxylic acids, *Tetrahedron Letters* 47 (2006) 4823-4826. Doi: 10.1016/j.tetlet.2006.05.052
- [11]. S.D. Düşünceli, D. Ayaz, E. Üstün, S. Günal, N. Özdemir, M. Dinçer, İ. Özdemir, Synthesis, antimicrobial properties, and theoretical analysis of benzimidazole-2-ylidene silver(I) complexes, *Journal of Coordination Chemistry* 73 (2020) 1967-1986. Doi: 10.1080/00958972.2020.1812587
- [12]. J. Valdez, R. Cedillo, A. Hernández-Campos, L. Yépez, F. Hernández-Luis, G. Navarrete-Vázquez, A. Tapia, R. Cortés, M. Hernández, R. Castillo, Synthesis and antiparasitic activity of 1H-benzimidazole derivatives, *Bioorganic & Medicinal Chemistry Letters* 12 (2002) 2221-2224. Doi: 10.1016/S0960-894X(02)00346-3
- [13]. M. Tonelli, M. Simone, B. Tasso, F. Novelli, V. Boido, F. Sparatore, G. Paglietti, S. Pricl, G. Giliberti, S. Blois, C. Ibba, G. Sanna, R. Loddo, P. Colla, Antiviral activity of benzimidazole

- derivatives. II. Antiviral activity of 2-phenylbenzimidazole derivatives, *Bioorganic & Medicinal Chemistry* 18 (2010) 2937-2953. Doi: 10.1016/j.bmc.2010.02.037
- [14]. E. Üstün, A. Özgür, K.A. Coşkun, S.D. Düşünceli, İ. Özdemir, Y. Tutar, Anticancer activities of manganese-based photoactivatable CO-releasing complexes (PhotoCORMs) with benzimidazole derivative ligands, *Transition Metal Chemistry* 42 (2017) 331–337. Doi: 10.1007/s11243-017-0136-x
- [15]. M. Gaba, S. Singh, C. Mohan, Benzimidazole: An emerging scaffold for analgesic and anti-inflammatory agents, *European Journal of Medicinal Chemistry* 76 (2014) 494-505. Doi: 10.1016/j.ejmech.2014.01.030
- [16]. J. Velík, V. Baliharová, J. Fink-Gremmels, S. Bull, J. Lamka, L. Skálová, Benzimidazole drugs and modulation of biotransformation enzymes, *Research in Veterinary Science* 76 (2004) 95-108. Doi: 10.1016/j.rvsc.2003.08.005
- [17]. A.G. Saimot, A.C. Cremieux, J.M. Hay, A. Meulemans, M.D. Giovanangeli, B. Delaitre, J.P. Coulaud, Albendazole as a potential treatment for human hydatidosis, *The Lancet* 322 (1983) 652-656. Doi: 10.1016/S0140-6736(83)92533-3
- [18]. R.R. Nadendla, Molecular modeling: A powerful tool for drug design and molecular docking, *Resonance* 9 (2004) 51–60. Doi: 10.1007/BF02834015
- [19]. J.C. Phillips, Generalized Koopmans' Theorem, *Phys. Rev.* 123, 420. Doi: 10.1103/PhysRev.123.420
- [20]. <https://www.rcsb.org/structure/2GTB> (for 2gtb); <https://www.rcsb.org/structure/5R82> (for 5r82); <https://www.rcsb.org/structure/6W9C> (for 6w9c)
- [21]. T.W. Lee, M.M. Cherney, J. Liu, K.E. James, J.C. Powers, L.D. Eltis, M.N.G. James, Crystal structures reveal an induced-fit binding of a substrate-like aza-peptide epoxide to SARS coronavirus main peptidase, *J. Mol. Biol.* 366 (2007) 916-932. Doi: 10.1016/j.jmb.2006.11.078
- [22]. A. Douangamath, D. Fearon, P. Gehrtz, T. Krojer, P. Lukacik, C.D. Owen, E. Resnick, C. Strain-Damerell, A. Aimon, P. Abranyi-Balogh, J. Brandao-Neto, A. Carbery, G. Davison, A. Dias, T.D. Downes, L. Dunnett, M. Fairhead, J.D. Firth, S.P. Jones, A. Keeley, G.M. Keseru, H.F. Klein, M.P. Martin, M.E.M. Noble, P. O'Brien, A. Powell, R.N. Reddi, R. Skyner, M. Snee, M.J. Waring, C. Wild, N. London, F. von Delft, M.A. Walsh, Crystallographic and electrophilic fragment screening of the SARS-CoV-2 main protease, *Nat Commun* 11 (2020) 5047. Doi: 10.1038/s41467-020-18709-w
- [23]. J. Osipiuk, R. Jędrzejczak, C. Tesar, M. Endres, L. Stols, G. Babnigg, Y. Kim, K. Michalska, A. Joachimiak, The crystal structure of papain-like protease of SARS CoV-2, Center for Structural Genomics of Infectious Diseases, to be published.
- [24]. N. Şahin, G. Serdaroğlu, S. D. Düşünceli, M. N. Tahir, C. Arıcı, İ. Özdemir, Direct arylation of heteroarenes by PEPPSI-type palladium–NHC complexes and representative quantum chemical calculations for the compound which the structure was determined by X-ray crystallography, *Journal of Coordination Chemistry* 72 (2019) 3258-3284. Doi: 10.1080/00958972.2019.1692202.
- [25]. A.D. Becke, Density-functional exchange-energy approximation with correct asymptotic behavior. *Phys Rev A Gen Phys.* 38 (1988) 3098-3100. Doi: 10.1103/PhysRevA.38.3098.
- [26]. J.P. Perdew, K. Burke, M. Ernzerhof, Generalized Gradient Approximation Made Simple, *Phys. Rev. Lett.* 77 (1996) 3865-3868. Doi: 10.1103/PhysRevLett.77.3865
- [27]. D.A. Pantazis, X.Y. Chen, C.R. Landis, F. Neese, All-Electron Scalar Relativistic Basis Sets for Third-Row Transition Metal Atoms, *J. Chem. Theory Comput.* 4 (2008) 908-919. Doi: 10.1021/ct800047t
- [28]. C. Lee, W. Yang, R.G. Parr, Development of the Colle-Salvetti correlation-energy formula into a functional of the electron density, *Phys. Rev. B* 37 (1988) 785–789. Doi: /10.1103/PhysRevB.37.785
- [29]. F. Neese, The ORCA program system, *WIREs Computational Molecular Science* 2 (2011)73-78. Doi: 10.1002/wcms.81
- [30]. J. P. Perdew, Density-functional approximation for the correlation energy of the inhomogeneous electron gas, *Phys. Rev. B.* 33 (1986) 8822. Doi: 10.1103/PhysRevB.33.8822
- [31]. F. Weigend, R. Ahlrichs, Balanced basis sets of split valence, triple zeta valence and quadruple zeta valence quality for H to Rn: Design and assessment of accuracy, *Phys. Chem. Chem. Phys.* 7 (2005) 3297–3305. Doi: /10.1039/B508541A
- [32]. G.M. Morris, R. Huey, W. Lindstrom, M.F. Sanner, R.K. Belew, D.S. Goodsell, A.J. Olson, Autodock4 and AutoDockTools4: automated docking with selective receptor flexibility, *J. Computational Chemistry* 16 (2009) 2785-2791. Doi: 10.1002/jcc.21256
- [33]. U.C. Singh, P.A. Kollman, An approach to computing electrostatic charges for molecules, *Journal of Computational Chemistry* 5 (1984) 129-145. Doi: 10.1002/jcc.540050204
- [34]. B.D. Bursulaya, M. Totrov, R. Abagyan, C.L. Brooks, Comparative study of several algorithms for flexible ligand docking, *Journal of Computer-Aided Molecular Design* 17 (2004) 755–763. Doi: 10.1023/B:JCAM.0000017496.76572.6f
- [35]. G.M. Morris, D.S. Goodsell, R.S. Halliday, R. Huey, W.E. Hart, R.K. Belew, A.J. Olson, Automated docking using a Lamarckian genetic algorithm and an empirical binding free energy function, *Journal of Computational Chemistry* 19 (1999) 1639-1662. Doi: 10.1002/(SICI)1096-987X(19981115)19:14<1639::AID-JCC10>3.0.CO;2-B
- [36]. BIOVIA, Dassault Systèmes, Discovery Studio, [4.1.0], San Diego: Dassault Systèmes, [2019].
- [37]. G. Serdaroğlu, N. Şahin, The synthesis and characterization of 1-(Allyl)-3-(2-methylbenzyl) benzimidazolium chloride: FT-IR, NMR, and DFT computational investigation, *Journal of Molecular*

- Structure 1178 (2019) 212-221. Doi: 10.1016/j.molstruc.2018.10.028
- [38]. N. Uludağ, G. Serdaroglu, An improved synthesis, spectroscopic (FT-IR, NMR) study and DFT computational analysis (IR, NMR, UV-Vis, MEP diagrams, NBO, NLO, FMO) of the 1,5-methanoazocino[4,3-b]indole core structure, Journal of Molecular Structure 1155 (2018) 548-560. Doi: 10.1016/j.molstruc.2017.11.032
- [39]. M.M.L. Kadam, D. Patil, N. Sekar, 4-(Diethyl-amino) salicylaldehyde based fluorescent Salen ligand with red-shifted emission – A facile synthesis and DFT investigation, Journal of Luminescence 204 (2018) 354-367. Doi: 10.1016/j.jlumin.2018.08.040
- [40]. R. Vijayaraj, V. Subramanian, P.K. Chattaraj, Comparison of Global Reactivity Descriptors Calculated Using Various Density Functionals: A QSAR Perspective, J. Chem. Theory Comput. 5 (2009) 2744–2753. Doi: 10.1021/ct900347f
- [41]. M. Berkowitz, R.G. Parr, Molecular hardness and softness, local hardness and softness, hardness and softness kernels, and relations among these quantities, J. Chem. Phys. 88 (1988) 2554. Doi: 10.1063/1.454034
- [42]. R.G. Parr, L. Szentpály, S. Liu, Electrophilicity Index, Am. Chem. Soc. 121 (1999) 1922–1924. Doi: 10.1021/ja983494x
- [43]. B. Salim, M. Nouredine, Identification of Compounds from Nigella Sativa as New Potential Inhibitors of 2019 Novel Coronasvirus (Covid-19): Molecular Docking Study, ChemRxiv. Cambridge: Cambridge Open Engage, (2020). Doi: 10.26434/chemrxiv.12055716.v1
- [44]. A.A. Al-Zahrani, Rutin as a Promising Inhibitor of Main Protease and Other Protein Targets of COVID-19: In Silico Study, Nat. Prod. Commun. 15 (2020) 1–4. Doi: 10.1177/1934578X20953951

Received: 02.06.2021

Received in revised form: 14.12.2021

Accepted: 15.12.2021